Preventing tumor escape by targeting a post-proteasomal trimming independent epitope

Ana Textor,[1] Karin Schmidt,[1,2] Peter-M. Kloetzel,[2,3] Bianca Weißbrich,[4] Cynthia Perez,[1] Jehad Charo,[1] Kathleen Anders,[1] John Sidney,[5] Alessandro Sette,[5] Ton N.M. Schumacher,[6] Christin Keller,[2] Dirk H. Busch,[4] Ulrike Seifert,[2,7,8] and Thomas Blankenstein[1,3,9]

[1]Max-Delbrück-Center for Molecular Medicine, 13125 Berlin, Germany
[2]Institute for Biochemistry, Charité, Campus Mitte, 10117 Berlin, Germany
[3]Berlin Institute of Health, 10117 Berlin, Germany
[4]Institute for Medical Microbiology, Immunology and Hygiene, Technical University, 81675 Munich, Germany
[5]La Jolla Institute for Allergy and Immunology, La Jolla, CA 92037
[6]The Division of Immunology, The Netherlands Cancer Institute, 1066 CX Amsterdam, Netherlands
[7]Institute for Molecular and Clinical Immunology, Otto-von-Guericke-Universität, 39120 Magdeburg, Germany
[8]Friedrich Loeffler Institute of Medical Microbiology, University Medicine Greifswald, 17475 Greifswald, Germany
[9]Institute of Immunology, Charité, Campus Buch, 13125 Berlin, Germany

Adoptive T cell therapy (ATT) can achieve regression of large tumors in mice and humans; however, tumors frequently recur. High target peptide–major histocompatibility complex-I (pMHC) affinity and T cell receptor (TCR)–pMHC affinity are thought to be critical to preventing relapse. Here, we show that targeting two epitopes of the same antigen in the same cancer cells via monospecific T cells, which have similar pMHC and pMHC-TCR affinity, results in eradication of large, established tumors when targeting the apparently subdominant but not the dominant epitope. Only the escape but not the rejection epitope required postproteasomal trimming, which was regulated by IFN-γ, allowing IFN-γ–unresponsive cancer variants to evade. The data describe a novel immune escape mechanism and better define suitable target epitopes for ATT.

INTRODUCTION

Adoptive T cell therapy (ATT) can be highly effective in treating individuals with late stage cancer. Treating metastatic melanoma with in vitro expanded tumor-infiltrating lymphocytes achieved objective response rates (49–72%), depending on the preconditioning regimen (Rosenberg et al., 2011). This represents one of the most effective therapies of metastatic melanoma for patients amenable to ATT. Nevertheless, in 74/93 patients, tumors recurred within 3 yr after treatment (Rosenberg et al., 2011). Tumor recurrence can be attributed to the transferred T cells, the cancer, or the host. Metastatic melanoma trials suggested loss of the target antigen (Melan-A/Mart-1) as escape mechanism (Yee et al., 2002; Mackensen et al., 2006), likely because of the poor binding of Melan-A/Mart-1 epitope to MHC class I (MHC-I) restriction element (HLA-A*0201), a factor that predicts tumor escape (Engels et al., 2013). In other cases, loss of the *β2-microglobulin* (*β2m*) gene and concomitant loss of MHC-I cell surface expression was suggested (Restifo et al., 1996; Paschen et al., 2003; Chang and Ferrone, 2007). The *β2m* gene is in close vicinity to a tumor suppressor gene frequently deleted in cancer (15q21.1; Feenstra et al., 1999; Leal et al., 2008), and loss of MHC-I appears to confer a growth advantage for cancer cells unrelated to immune effects (Garrido et al., 2012). Therefore, it is unclear whether MHC-related genetic lesions are the result of immune escape or simply increased malignancy. Such a cause-and-effect relationship is difficult to address in the clinic, mainly because of the limited number of patients in which the T cell pressure might be sufficiently strong and persistent that the cancer cells indeed needed to escape. In most cases, the transferred T cells were specific for self-antigens and derived from the autologous repertoire, skewed toward low-avidity T cells (Lyman et al., 2005).

Cancer cells could evade T cell recognition by several other mechanisms. Defects in the proteasome or transporter associated with antigen processing could cause altered or impaired peptide generation (Androlewicz et al., 1993; Rock et al., 1994; Suh et al., 1994). IFN-γ responsiveness by the cancer cells favors their rejection (Dighe et al., 1994; Kaplan et al., 1998). It also increases MHC-I expression and induces components of the immunoproteasome, leading to a broader peptide pool (Kloetzel and Ossendorp, 2004). However, many MHC-I ligands are produced in the form of extended precursors that require the removal or trimming of amino acids to adapt to the constraints of the MHC-I peptide-binding site (Weimershaus et al., 2013). This trimming is mainly per-

Correspondence to Thomas Blankenstein: tblanke@mdc-berlin.de

Abbreviations used: Ab, antibody; ATT, adoptive T cell therapy; ERAAP, endoplasmic reticulum–resident aminopeptidase; MS, mass spectrometry; pI, peptide I; pIV, peptide IV; pMHC, peptide-MHC; WB, Western blot.

The Rockefeller University Press $30.00
J. Exp. Med. 2016 Vol. 213 No. 11 2333–2348
www.jem.org/cgi/doi/10.1084/jem.20160636

The Journal of Experimental Medicine

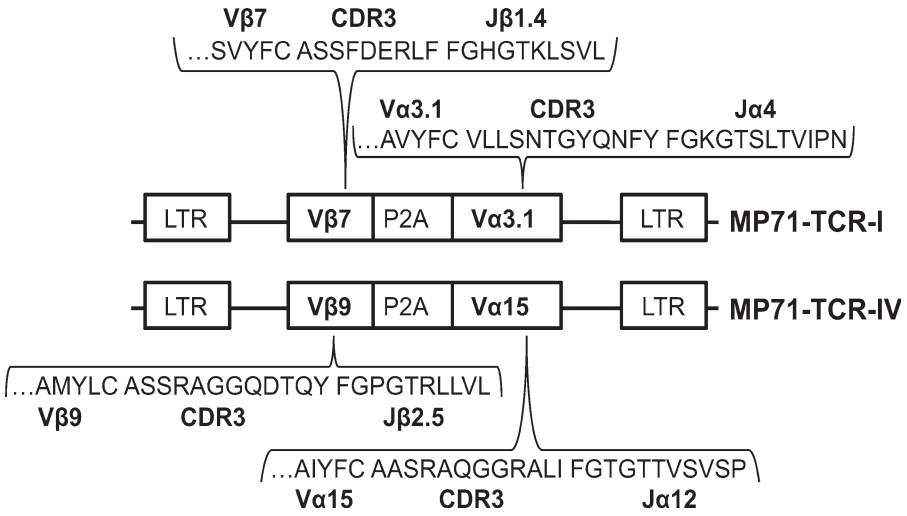

Figure 1. **Schematic representation of TCR-I and TCR-IV retroviral vectors with both TCR chains linked by a P2A element as indicated.**

formed by the endoplasmic reticulum–resident aminopeptidase ERAAP (the human homologue is ERAP1), which is also IFN-γ inducible (Saric et al., 2002; Serwold et al., 2002).

Target cell recognition by T cells is the result of a tripartite interaction between the peptide, the presenting MHC molecule, and the TCR. Targeting peptide–MHC-I complexes (pMHC) with high affinity led to eradication of large established tumors, whereas targeting pMHC with low affinity selected antigen loss variants (Engels et al., 2013). Similarly, high but not low TCR affinity for pMHC resulted in effective T cell responses with high affinity TCRs typically deriving from the nontolerant and low affinity TCRs from the tolerant repertoire (Theobald et al., 1995). Thus, if pMHC and pMHC-TCR affinities were similar for two peptide epitopes, T cells might be similarly effective or ineffective in rejecting tumors. Therefore, it was critical when comparing the usefulness of different peptide epitopes as targets for ATT to keep the model constant for all but one factor. To this end, we introduced TCRs into monospecific TCR transgenic $CD8^+$ T cells specific for an antigen not expressed by the host or the cancer cells, which ensured that the $CD8^+$ T cells redirected with different TCRs had identical phenotype at the time of transfer. The TCRs were originally isolated from antigen-negative hosts, i.e., the unskewed repertoire. By targeting two different epitopes of the same tumor antigen in the same cancer cells, we excluded the amount of antigen, frequency of variant clones, and tumor-induced immune suppression as possible factors for differential immune escape. Arguably, genetic instability of cancer cells and tumor burden are the highest risk factors for immune escape. Therefore, we treated tumors grown for several weeks to ∼1 cm diam (∼500 mm^3), which corresponds to a clinically detectable mass of $\sim 10^9$ tumor cells (Yu et al., 2006).

We targeted two different epitopes of SV40 large T (T-Ag) in tumors whose growth depended on T-Ag (Anders and Blankenstein, 2013). The H2-K^b–presented peptide IV (pIV) is dominant, with ∼11% of the $CD8^+$ T cells in T-Ag immunized wild-type mice being pIV specific, demonstrating that the epitope is efficiently processed and presented under vaccine conditions (Mylin et al., 2000). The H2-D^b–presented peptide I (pI) is sub-dominant, with ∼3% specific $CD8^+$ T cells at peak levels. Nevertheless, pI-specific $CD8^+$ T cells can eradicate large established tumors (Anders et al., 2011; Charo et al., 2011) and pIV-specific $CD8^+$ T cells were shown to control autochthonous pancreatic or prostate carcinomas (Garbi et al., 2004; Otahal et al., 2007; Bendle et al., 2013). However, in these cases tumor burden at the time of ATT was probably too low to allow for the generation of escape variants. Here, we show that pI and pIV bind with similar affinity to MHC-I, and that pI- and pIV-specific TCR-redirected $CD8^+$ T cells (TCR-I and TCR-IV, respectively) have similar affinity to the cognate pMHC. Both rejected large established tumors expressing high amounts of MHC-I molecules but tumors with low MHC-I were eradicated only by TCR-I T cells. TCR-IV T cells selected IFN-γ–unresponsive escape variants, which was possible because pIV, but not pI, required postproteasomal trimming by ERAAP for efficient T cell recognition, suggesting that IFN-γ–independent epitopes are better targets for ATT.

RESULTS

TCR-I and TCR-IV redirected T cells have similar avidity

To maximize the correct chain pairing and surface expression upon T cell transduction, the α and β genes of TCR-I and TCR-IV, respectively, were connected by the P2A element (β-P2A-α), codon optimized, and integrated into retroviral vectors (Fig. 1). To generate monospecific T cells, TCR-transgenic $CD8^+$ T cells derived from $Rag^{-/-}$ mice specific for lymphocytic choriomeningitis virus gp33 (P14) or ovalbumin (OT-1) were transduced with TCR-I or TCR-IV. Both TCRs were equally well expressed (Fig. 2 A). The mean expression on $CD8^+$ T cells derived from P14 mice was 76%

(SD ± 3%; n = 4) and 77% (SD ± 3%; n = 4) for TCR-I and TCR-IV, respectively. The expression levels, although similar between the two TCRs, were generally lower on OT-1 T cells (46%; SD ± 18% for TCR-I; n = 4; and 40%; SD ± 16% for TCR-IV; n = 4). We next compared the avidity of TCR-I and TCR-IV T cells by labeling them with pMHC multimers, which can be dissociated into monomers, termed MHC *Strep*tamers. The dissociation of MHC *Strep*tamers from the T cell surface accurately measures k_{off}-rates and was followed by confocal microscopy (Nauerth et al., 2013). The pMHC k_{off}-rate was comparable for the two TCRs (36 s, SD ± 13 s for TCR-I; 46 s, SD ± 7 s for TCR-IV); if anything, the $T_{1/2}$ was longer for TCR-IV T cells (P = 0.002; Fig. 2 B). When we compared the functional avidity of TCR-I and TCR-IV T cells by measuring the levels of secreted IFN-γ upon recognition of peptide-loaded, transporter associated with antigen processing–deficient RMA-S cells, we found that both TCR-I and TCR-IV T cells recognized lower peptide concentrations equally well (Fig. 2 C). These data exclude differences in TCR affinity as a major variable in our system.

Tet-TagLuc and 16.113p cells have similar T-Ag levels, whereas pI and IV have similar pMHC affinity and pMHC-I levels on the cell surface

To characterize the two T-Ag$^+$ cancer cell lines used in this study, Tet-TagLuc and 16.113p (Anders et al., 2011; Charo et al., 2011), we evaluated factors that can influence the likelihood of tumor recurrence, such as pMHC affinity (Spiotto et al., 2004; Engels et al., 2013) and antigen expression levels. Tet-TagLuc and 16.113p cells expressed similar levels of T-Ag (Fig. 3 A). The affinity of pI and pIV for MHC-I was analyzed in a cell-free peptide competition assay. The peptide concentrations needed for replacing 50% of the indicator peptides bound to H2-D^b and H2-K^b, respectively, were quite similar (IC_{50}, 31 and 76 nM for pI and pIV, respectively; Fig. 3 B). Because the functional avidity was similar for TCR-I and TCR-IV T cells (Fig. 2 C), co-culturing these T cells with T-Ag$^+$ cancer cells could indirectly answer whether the two epitopes are equally well presented on the cancer cell surface. To maximize the surface expression of pI and pIV, we stimulated Tet-TagLuc and 16.113p cells with IFN-γ for 48 h. TCR-I and TCR-IV T cells recognized both cell lines equally well (Fig. 3 C), thus we conclude that the levels of surface expression was similar for both epitopes.

TCR-I and TCR-IV T cells reject Tet-TagLuc tumors, but 16.113p tumors escape TCR-IV T cell pressure

Because MHC-I expression influences the amount of peptide presented on the cell surface, we analyzed MHC-I expression by Tet-TagLuc and 16.113p cells. MHC-I expression (H2-K^b/D^b) was lower for 16.113p (Kb/Db MFI, 10.5/4.8; SD ± 9.9/2.3; n = 3) compared with Tet-TagLuc cells (Kb/Db MFI, 21.9/14.7; SD ± 21.3/6.3; n = 3), even after IFN-γ stimulation (Kb/Db MFI, 79.3/30; SD ± 60.9/10.8 and 162.5/62.1 SD ± 137.1/29.4; n = 3, for 16.113p and

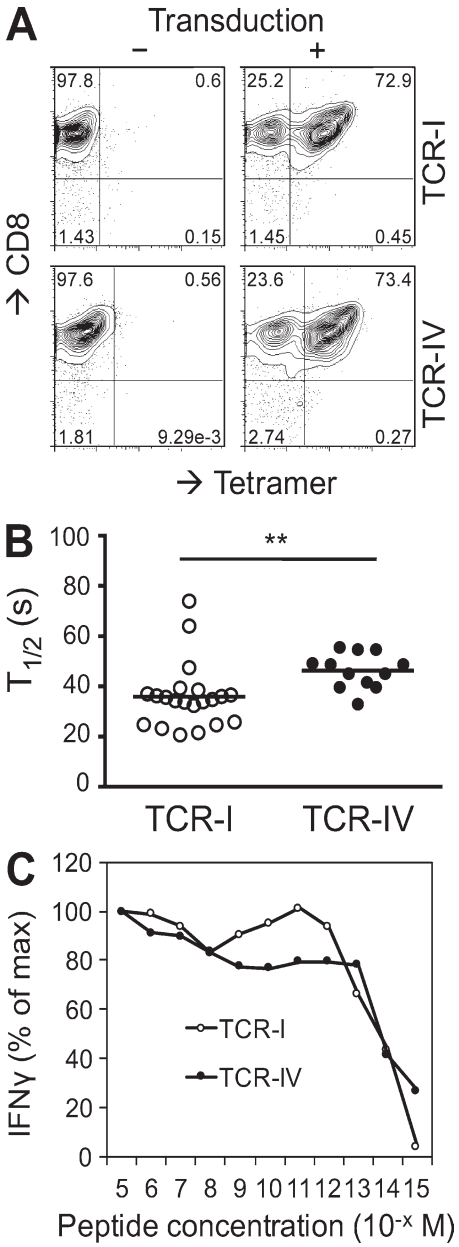

Figure 2. **Similar avidity for TCR-I and TCR-IV T cells.** (A) Untransduced and TCR-I– or TCR-IV–transduced CD8$^+$ P14/Rag$^{-/-}$ T cells labeled with pI- or pIV-specific tetramers and gated on total lymphocytes. One representative of four experiments is shown. (B) The time needed for dissociation of 50% of bound pMHC complexes ($T_{1/2}$) from the surface of an individual T cell is indicated in seconds (TCR-I, n = 21; TCR-IV, n = 12). Combined data from two experiments. The two datasets were compared using a two-sided Wilcoxon rank sum test (P = 0.002). (C) IFN-γ values obtained by co-culturing TCR-I and TCR-IV T cells with equal numbers of RMA-S cells pulsed with different concentrations of pI or pIV. The values are given as percentage of maximum, which was calculated by taking the T cell response to the highest peptide concentration as 100% (maximal value), and then calculating the percentage of for each value as percentage of maximum. One representative experiment of two is shown.

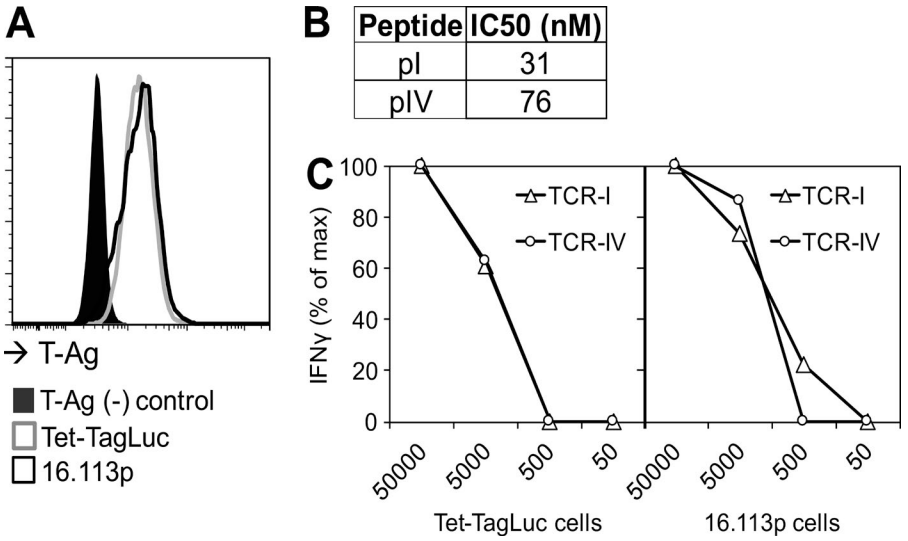

Figure 3. **Similar Ag levels for Tet-TagLuc and 16.113p cells, and similar pMHC affinity for pI and pIV.** (A) Histogram shows T-Ag expression measured in T-Ag–negative cells (MCA-205), Tet-TagLuc, and 16.113p tumor cells by intracellular T-Ag staining. One representative of two experiments is shown. (B) The concentration of pI and pIV necessary for yielding 50% binding inhibition (IC_{50}) of the indicator peptides to MHC-I (pI/H2-D^b, pIV/H2-K^b). One representative of three experiments is shown. (C) IFN-γ values obtained by 24-h co-culturing of 10^5 TCR-I or TCR-IV T cells with indicated numbers of Tet-TagLuc or 16.113p tumor cells. The target cells were incubated with 100 ng/48 h IFN-γ before co-culture. The values are given as percentage of maximum, which was calculated by taking the T cell response to the highest tumor cell number as 100% (maximal value), and then calculating the percentage of for each value as percentage of maximum. One representative of two experiments is shown.

Tet-TagLuc, respectively; Fig. 4 A). To analyze whether the difference in MHC-I has an impact on ATT depending on the targeted epitope, we compared the ability of TCR-I and TCR-IV T cells to reject large, established Tet-TagLuc and 16.113p tumors. $Rag^{-/-}$ mice bearing ∼4-wk-old established Tet-TagLuc or 16.113p tumors received 5×10^4 TCR-I, TCR-IV, or mock T cells. The mean tumor volume at the day of treatment was ∼500 mm^3 (497 mm^3; SD ± 111 mm^3) for Tet-TagLuc and ∼400 mm^3 (358 mm^3; SD ± 60 mm^3) for 16.113p tumors. Tet-TagLuc tumors were rejected in all cases

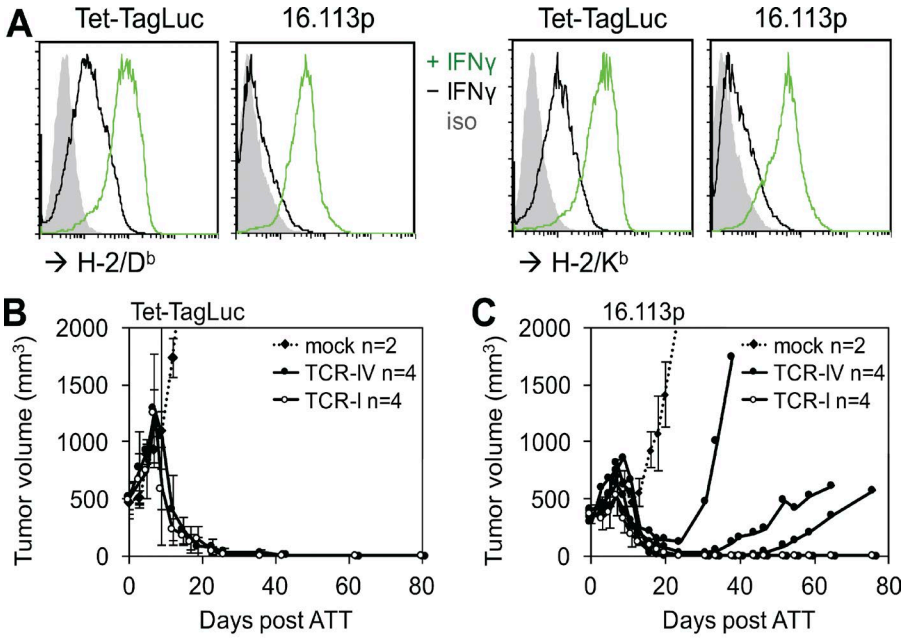

Rejection:

TCR-I	TCR-IV	mock
11/11	11/11	0/9

Total mice from 4 experiments

Rejection:

TCR-I	TCR-IV	mock
17/17	4/16	0/11

Total mice from 5 experiments

Figure 4. **TCR-I and TCR-IV T cells reject MHC-I high Tet-TagLuc tumors, but only TCR-I reject MHC-I low 16.113p, whereas TCR-IV T cells favor escape.** (A) H2-D^b and H2-K^b surface expression for Tet-TagLuc and 16.113p tumor cells stimulated with IFN-γ or left untreated and corresponding isotype controls are shown in the histograms. One representative of three experiments is shown. (B) Tet-TagLuc tumor volumes over time for $Rag^{-/-}$ mice receiving TCR-I, TCR-IV, or mock-transduced P14/$Rag^{-/-}$ $CD8^+$ T cells. Each line represents the mean value of indicated numbers of mice receiving the same therapy. Error bars correspond to SD. Total mouse numbers from four experiments are shown in the table. (C) 16.113p tumor volumes of indicated number of $Rag^{-/-}$ mice are shown for TCR-I and mock (error bars correspond to SD), and each line represents a single mouse for TCR-IV (n = 4) treatment. Total mouse numbers from five experiments are shown in the table.

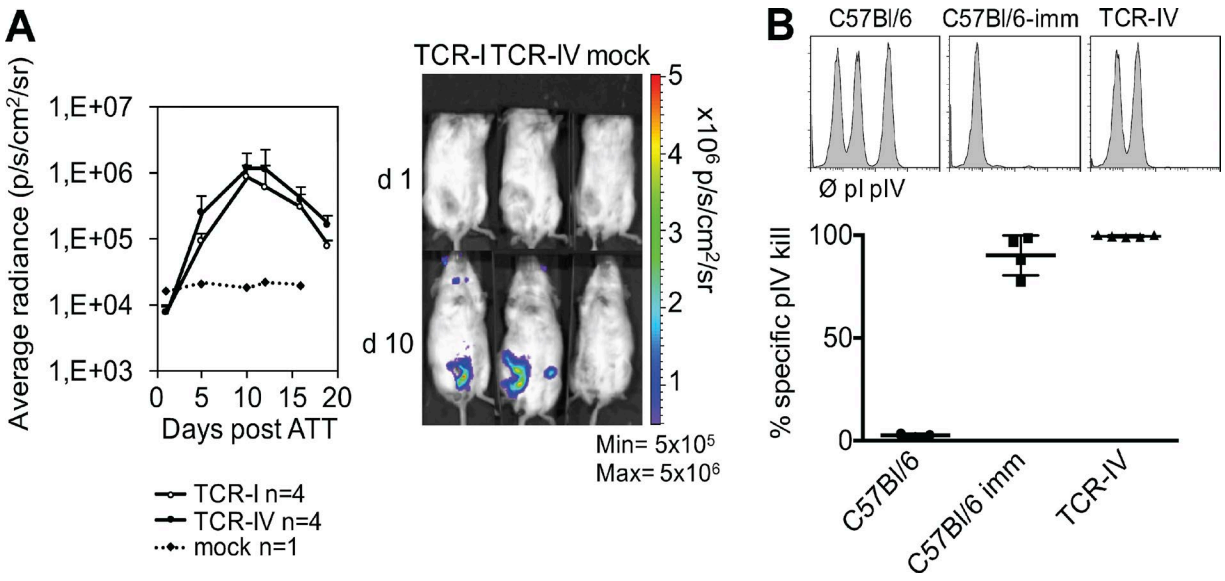

Figure 5. **TCR-IV T cells remain functional in mice with tumor escape.** (A) Mean radiance of the signal emitted at the tumor site by localized T cells over time. T cell signal curves for mice receiving TCR-I– and TCR-IV–transduced ChRLuc/OT-1/Rag$^{-/-}$ CD8^{+} T cells represent a mean of four mice, and one mouse for mock. Error bars correspond to SD. One representative mouse for each treatment is shown at days 1 and 10 after ATT. One representative experiment out of three is shown. (B) The histograms depict three peptide-pulsed CD45.1^{+} gated splenocyte populations (no peptide, pI, and pIV) with low, intermediate, and high CFSE concentration. C57BL/6 mice that were either immunized with 16.113 cells 1 wk before the experiment or left untreated, and a TCR-IV–treated Rag$^{-/-}$ mouse with recurrent 16.113p tumor (TCR-IV), are shown. The specific pIV kill of individual mice for each group is shown in the chart below the histograms (n = 3 for C57BL/6; n = 4 for C57BL/6 imm; n = 5 for TCR-IV).

by TCR-I and TCR-IV T cells, whereas in mock-treated mice tumors progressed (Fig. 4 B). In contrast, TCR-I T cells eradicated 16.113p tumors, whereas in 3/4 mice receiving TCR-IV T cells tumors eventually relapsed after initial regression (Fig. 4 C). In total, 12/16 16.113p tumors recurred in TCR-IV T cell-treated mice and in 0/17 mice receiving TCR-I therapy (Fig. 4 C), suggesting that pMHC and pMHC-TCR affinities are not sufficient parameters to predict rejection epitopes. We next investigated whether TCR-IV T cell tumor recognition was impaired in vivo. We treated 16.113p tumor-bearing mice with Renilla Luciferase (RLuc) expressing TCR-I and TCR-IV T cells (Charo et al., 2011) to monitor T cell accumulation at the tumor site by bioluminescent imaging. The signal for both TCR-I and TCR-IV T cells appeared at a similar time in the tumor and peaked at day 10 (Fig. 5 A), indicating that tumor infiltration and proliferation of TCR-IV T cells was not impaired. To examine whether TCR-IV T cells were still functional in mice with recurrent tumor, we performed an in vivo kill assay. We injected those mice with unpulsed and pI- and pIV-pulsed splenocytes labeled with different CFSE concentrations and, after 16 h, analyzed for specific kill of pIV-pulsed population. Naive and 16.113-immunized C57BL/6 mice served as negative and positive controls. Unlike naive mice, immunized C57BL/6 mice effectively killed both pI- and pIV-pulsed but not unpulsed cells. The specific pIV kill was 2.6% (SD ± 0.9%; n = 3) for naive and 90.1% (SD ± 9.7%; n = 4) for immunized C57BL/6 mice (Fig. 5 B). TCR-IV T cells in mice with recurrent 16.113p tumors were still functional, as they lysed the pIV-pulsed splenocytes with 99.5% (SD ± 0.5%; n = 5) specific kill (Fig. 5 B), but not pI-pulsed or unpulsed splenocytes.

16.113p tumors escape TCR-IV T cells by disrupted IFN-γ signaling

Because TCR-IV T cells remained functional despite progressively growing tumors, seven escape variants were isolated from TCR-IV T cell–treated mice and analyzed for the mechanism of escape. We analyzed them for MHC-I and IFN-γ receptor (IFNγR) expression, and several other IFN-γ–inducible genes, and all seven escape variants showed similar results. The expression of H-2/D^{b} and K^{b} molecules on the escape variants was lower when compared with the parental 16.113p cells and could not be clearly detected with individual antibodies (Fig. S1 A). Therefore, we amplified the MHC-I signal by using biotinylated pan MHC-I (anti-H-2/D^{b}/K^{b}) antibody (Ab) and fluorochrome-coupled streptavidin. Without IFN-γ stimulation, MHC-I expression was a bit lower for the 999 escape variant compared with the parental 16.113p cells (16.113p/999 MFI: 56.6/18.8; SD ± 2.8/1.7; n = 2; Fig. 6 A). Upon IFN-γ stimulation, only parental 16.113p cells up-regulated MHC-I expression (16.113p/999 MFI: 547/18.6; SD ± 124.5/0.8; n = 2), indicating that variants with acquired IFN-γ unresponsiveness had been selected under TCR-IV T cell pressure (Fig. 6 A and Fig. S1 B). Despite the IFN-γ unresponsiveness, 999 cells still expressed the IFNγR (16.113p/999 MFI, 1,214/1,924.5; SD ± 687.3/1,966.5; n =

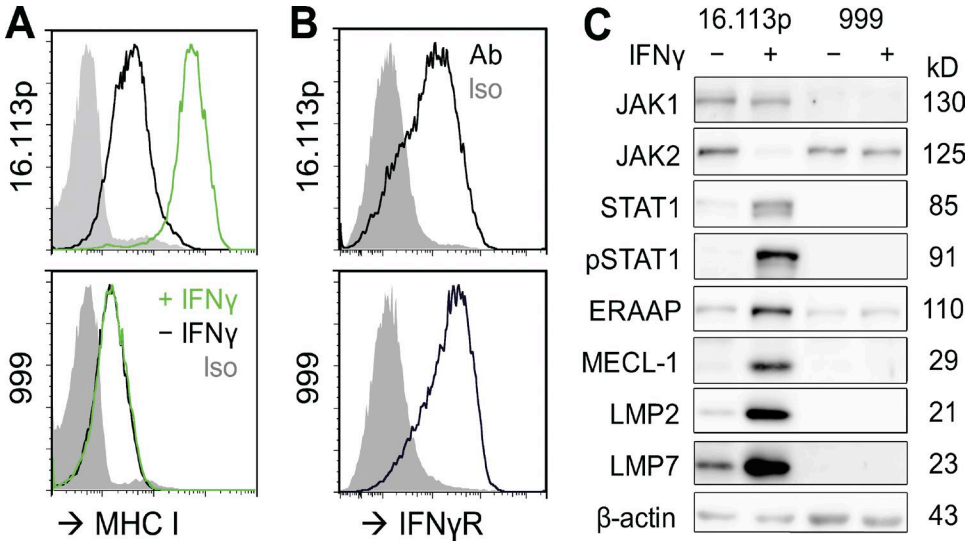

Figure 6. **TCR-IV escape variants are unresponsive to IFN-γ stimulation.** (A) Shown in the histograms is the MHC-I expression by double staining with biotin-α-H2-K^b/D^b and streptavidin Ab, including the corresponding isotype controls for untreated or IFN-γ–pretreated (100 ng/48 h) 16.113p and 999 (escape variant) cells. One representative staining of two is shown. All seven escape variants were analyzed with similar results (Fig. S1 B). (B) Shown in the histograms is the IFNγR expression on 16.113p and 999 cells by double staining with biotin-α-CD119 Ab and streptavidin Ab, including the corresponding isotype control. The signal was amplified using FASER kit. Shown is one representative staining of two. All seven escape variants were analyzed with similar results (Fig. S1 C). (C) A WB for indicated proteins that were isolated from 16.113p and 999 cells, with or without IFN-γ pretreatment (100 ng/48 h). The same blot was repeatedly stripped and rehybridized. One representative of two is shown, and the blots for the other escape variants are shown in Fig. S2 (A and B).

2; Fig. 6 B), and so did the other TCR-IV escape variants (Fig. S1 C). We next analyzed the expression of several IFN-γ-inducible genes involved in antigen processing and presentation (β1i/LMP2, β5i/LMP7, β2i/MECL-1, and ERAAP) by Western blots (WBs). In contrast to parental 16.113p cells, none of the proteins were up-regulated in the 999 cells treated with IFN-γ for 48 h (Fig. 6 C). Thus, the escape variants had acquired a defect in the IFN-γ signaling pathway, which allowed 16.113p tumors to escape TCR-IV T cell therapy. Both STAT1 and phosphorylated STAT1 (pSTAT1) were detectable in the parental 16.113p cells, but not in 999 cells (Fig. 6 C), which suggests that the breakage in the IFN-γ signaling occurred further upstream in the cascade. Ligand-induced dimerization of IFN-γ receptor leads to JAK1 and JAK2 activation and phosphorylation of STAT1. JAK1 was still present in IFN-γ–stimulated 16.113p cells, whereas JAK2 was down-regulated (Fig. 6 C). These observations are in line with findings that IFN-γ also triggers a negative regulation loop by proteasomal targeting of ubiquitinated JAK2 (Ungureanu et al., 2002). In the 999 cells, JAK2 was still present and JAK1 was completely down-regulated, indicating that the signaling cascade was disrupted at the level of JAK1, which had been observed before in human cancer cells (Dunn et al., 2005; Fig. 6 C). The WB of proteins for the IFN-γ–inducible genes and JAKs from the cell lysates of other escape variants are shown in Fig. S2 (A and B).

Recognition of pIV, but not pI, is dependent on IFN-γ signaling

To understand why the IFN-γ–unresponsive escape variants occurred only upon TCR-IV, but not TCR-I, T cell therapy, we analyzed their recognition by TCR-I and TCR-IV T cells in vitro and in vivo. For in vitro recognition, the parental 16.113p cell line and seven escape variants were incubated with TCR-I or TCR-IV T cells. In contrast to parental 16.113p cells, the recognition of the escape variants was impaired for TCR-IV but not TCR-I T cells (Fig. 7 A and Fig. S2 C), indicating that unlike for pIV, the recognition of pI did not require IFN-γ signaling. TCR-IV T cells recognized 16.113p without IFN-γ pretreatment (Fig. 7 A), suggesting that a small amount of pIV was produced in the absence of IFN-γ, enough to stimulate the T cells to secrete IFN-γ and further stimulate epitope production, leading to better recognition and more IFN-γ secretion. To obtain independent evidence that pIV was dependent on IFN-γ, we treated mice bearing Tet-TagLuc tumors, which are normally rejected by TCR-IV T cells (Fig. 4 B), with IFNγ$^{-/-}$ TCR-IV T cells to ask whether under these conditions tumors escaped. Mice with ∼4-wk-old established tumors (309 mm^3; SD ± 216 mm^3) received 5 × 10^5 IFN-γ$^{-/-}$ TCR-I, IFN-γ$^{-/-}$ TCR-IV, or mock (OT-1) T cells. Tumors progressed in mock-treated cells and were rejected in most of the IFN-γ$^{-/-}$ TCR-I T cell–treated mice (1/5 mice had a late relapse; Fig. 7 B). In contrast, Tet-TagLuc tumors in IFN-γ$^{-/-}$ TCR-IV T cell–treated mice regressed, in some cases completely, but finally resumed growth in 6/7 mice (9/10 tumors from two experiments; Fig. 7 B), confirming the critical role of IFN-γ for targeting pIV but not pI.

IFN-γ regulates pIV production through ERAAP

To elucidate the mechanism by which IFN-γ regulates pIV generation, we analyzed the processing of pI and pIV by the

constitutive proteasome and the immunoproteasome. No qualitative and no major quantitative differences were observed between the relevant cleavage products generated by either constitutive or immunoproteasomes (Fig. 8 and Fig. S3). Both, standard and immunoproteasome efficiently generated the T-Ag$_{206-215}$ epitope (pI) from T-Ag$_{196-221}$ polypeptide (Fig. 8 A and Fig. S3 A), and produced minor amounts of potential epitope precursor peptides plus the corresponding N-terminal flanking cleavage products (Fig. 8 A and Fig. S3 A). The precise minimal T-Ag$_{404-411}$ epitope (pIV) was difficult to detect and proteasomes generated only minor amounts of this minimal epitope (Fig. 8 B and Fig. S3 B). In contrast, N-terminally extended potential epitope precursor peptides plus their corresponding N-terminal flanking cleavage products were generated prominently (Fig. 8 B and Fig. S3 B). Additionally, we detected N-terminally extended cleavage products with methionine as C-terminal residue (Fig. 8 B and Fig. S3 B). This cleavage results indicated that efficient production of pIV required post-proteasomal trimming. Because up-regulation of ERAAP was impaired in the 16.113p escape variants (Fig. 6 C), we asked whether ERAAP was responsible for pIV generation. An escape variant was transduced with retrovirus containing ERAP1-GFP or only GFP, and GFP sorted. The GFP expression of sorted cells was stable over time for the cells that were transduced with GFP only, but not for ERAP1-GFP–transduced cells (Fig. 9 A). Therefore, three stably transduced clones were GFP selected from ERAP1-GFP–transduced cells, where clone 1 and 4 overexpressed ERAP1, whereas clone 2 was negative (Fig. 9 B). The GFP selected clones were similar to the original escape variant when other IFN-γ–inducible genes were compared (Fig. 9 B). We next compared the in vitro recognition of these cells by TCR-I and TCR-IV T cells. Because TCR-I T cells already recognize the original escape variants, introduction of ERAP1 in the escape variant did not affect TCR-I T cell recognition (Fig. 9 C). For TCR-IV T cells, the recognition of the escape variant was restored by introduction of ERAP1 (Fig. 9 C), demonstrating that ERAAP facilitates the IFN-γ–regulated generation of pIV. However, the levels of secreted IFN-γ were a bit lower in comparison to the values obtained upon recognition of parental 16.113p cells. This was not surprising considering that all the other IFN-γ–inducible proteins contributing to pMHC T cell recognition were still down-regulated in the selected clones.

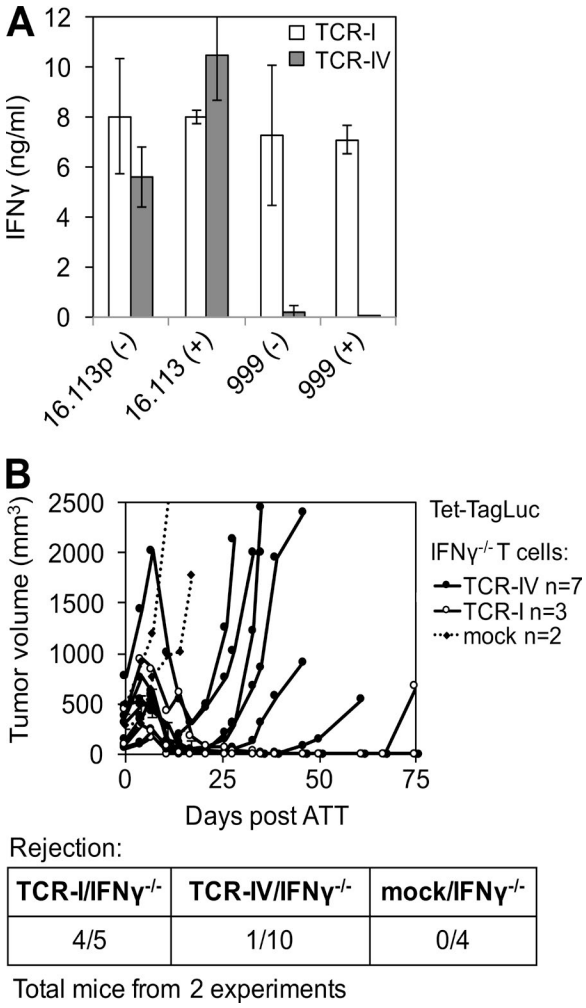

Rejection:

TCR-I/IFNγ$^{-/-}$	TCR-IV/IFNγ$^{-/-}$	mock/IFNγ$^{-/-}$
4/5	1/10	0/4

Total mice from 2 experiments

Figure 7. **Recognition of 16.113p escape variants by TCR-IV T cells is IFN-γ–dependent as well as the rejection of Tet-TagLuc tumors.** (A) Levels of secreted IFN-γ by TCR-I– or TCR-IV–transduced CD8$^+$ OT-1/Rag$^{-/-}$ T cells upon 24-h co-culture with 16.113p and 999 cells (with [+] or without [–] 100 ng/48 h IFN-γ pretreatment) measured by an IFN-γ ELISA assay (E:T/2:1). Combined data from two experiments are shown, and error bars indicate SD. The remaining escape variants from the same experiments are shown in Fig. S2 C. (B) Tumor volumes over time from Rag$^{-/-}$ mice bearing Tet-TagLuc tumors treated with TCR-I, TCR-IV, or mock T cells derived from OT-1/IFN-γ$^{-/-}$/Rag$^{-/-}$ mice. Each line reflects an individual mouse and the bottom table shows total mice numbers from two experiments.

IFN-γ–resistant variants appear only in established tumors despite the presence of endogenous T cells

Current models often use therapy a few days after cancer cell inoculation, which does not compare to tumors detected in the clinic. Assuming genetic instability and tumor burden as critical factors for generation of variants, we treated mice with 16.113p tumors grown for a short or long time period. Mice bearing large established tumors (533 mm^3; SD ± 293 mm^3) grown for ∼30 d or small tumors grown for ∼10 d (36 mm^3, SD ± 21 mm^3) were treated with 5 × 10^5 TCR-IV or mock T cells. In mock-treated mice, tumors progressed for both small and large tumors (Fig. 10 A). As expected, large established tumors regressed, but then recurred in all TCR-IV–treated mice; however, small 16.113p tumors were rejected and did not relapse during a 3-mo observation time (Fig. 10 A). These data suggest that variants occurred with low frequency and were present only in large tumors. Therefore, the IFN-γ–resistant variants likely also occurred in mice treated with TCR-I T cells, but were recognized and eliminated, which makes IFN-γ–independent epitopes better targets for ATT. Nevertheless, we cannot exclude

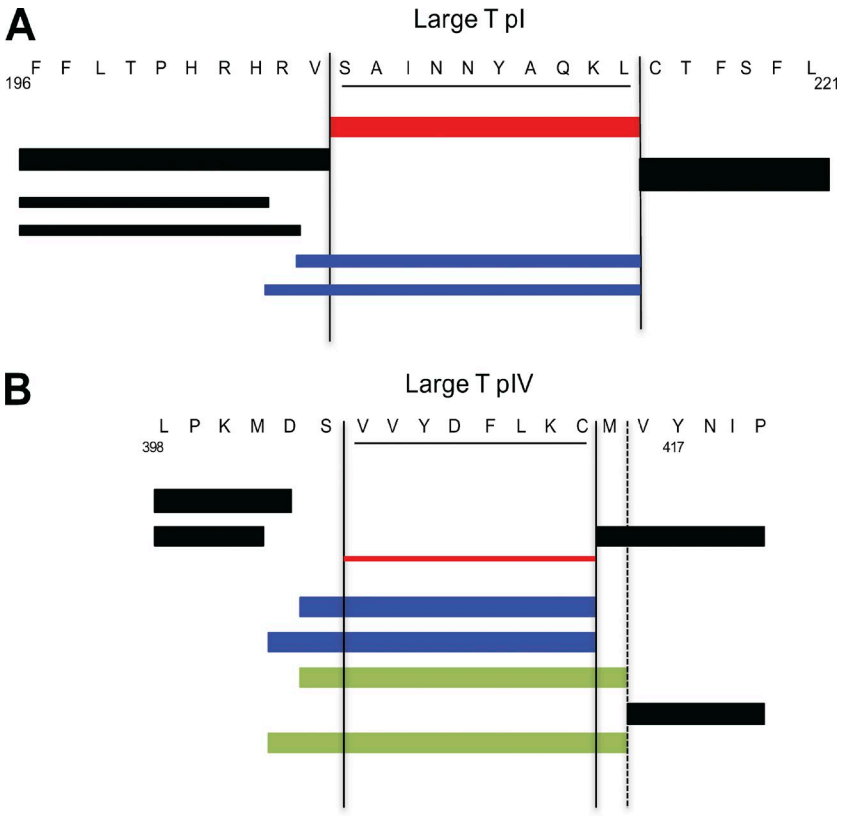

Figure 8. **Epitope I is produced in sufficient amounts by the proteasome, whereas epitope IV requires postproteasomal trimming.** Shown are the relevant cleavage products detected in standard proteasome digestions of T-Ag$_{196-221}$ (A) and T-Ag$_{398-417}$ (B) in three independent experiments. Irrelevant peptide-products are indicated in black, and the epitope and epitope precursor peptides are indicated in red and blue, respectively. For pIV, peptide precursors for an alternative epitope with methionine on the C terminus are shown in green. Thickness of the cleavage products indicates relative cleavage intensity.

the possibility that these variants would not have developed in the presence of functional endogenous T cells, as it is known that ERAP1 deficiency can lead to an altered peptide pool and immunogenicity (Hammer et al., 2007; James et al., 2013). To clarify this, we challenged T-Ag tolerant (LoxP-TagLuc-pA/CM2) mice (Buschow et al., 2010; Anders et al., 2012) with 16.113p cells to allow tumor growth in the presence of endogenous T cells. ∼3 wk later, when the tumors were large enough to possibly contain the variants (201.9 mm^3; SD ± 120.6 mm^3), mice were irradiated and treated with 5 × 10^5 TCR-IV T cells (one mouse received irradiation only). In the mouse which received irradiation only, the tumor progressed, whereas in the mice with irradiation and TCR-IV T cell transfer, tumors were rejected in 2/6 mice (Fig. 10 B). In the other four mice, tumors initially regressed, but later recurred (Fig. 10 B). We isolated those tumors and analyzed whether they were still responsive to IFN-γ. In 1/4 tumors, MHC-I expression was up-regulated upon IFN-γ stimulation (Fig. 10 C). It could be that the T cells became tolerant in this mouse because the LoxP-TagLuc-pA mice express low levels of T-Ag in normal tissues (Buschow et al., 2010). However, the remaining three tumors were IFN-γ unresponsive and could not up-regulate MHC-I (Fig. 10 C), demonstrating that similar escape variants also occur in immunocompetent mice.

DISCUSSION

As ATT becomes widely applicable and efficacy will continuously increase, tumor recurrence of escape variants will remain a major problem. Because too many factors can cause tumor recurrence, a reductionist approach is most suitable to firmly uncover the underlying mechanisms. Previous studies in which the peptide epitope was the only variable had shown that high pMHC affinity is a critical factor to prevent tumor recurrence (Engels et al., 2013). Compatible with these data, both pI and pIV with relatively high pMHC affinity served as rejection epitopes in the Tet-TagLuc tumor model. However, pMHC affinity was not sufficient to predict the "rejection epitope" when 16.113p tumors expressing low levels of MHC-I were targeted. TCR-I T cells targeting the subdominant epitope pI rejected large established tumors, whereas tumors in most cases escaped TCR-IV T cells targeting the dominant epitope pIV. Thus, immunodominance does not predict rejection epitopes, reminiscent of murine virus models, in which T cells against subdominant but not dominant epitopes were protective (Gallimore et al., 1998). In the clinic, mainly dominant epitopes have been targeted, because subdominant epitopes are difficult to identify.

Just as the antigen amount determines the efficiency of ATT, with higher antigen levels preventing tumor recurrence (Spiotto et al., 2004), the MHC-I level might have a similar role because the actual amount of the surface presented epitope is influenced by it (Cormier et al., 1999). With 16.113p cells inherently expressing lower levels of MHC-I, the TCR-IV T cells might not have acquired as much stimuli as with Tet-TagLuc tumors to produce enough effector

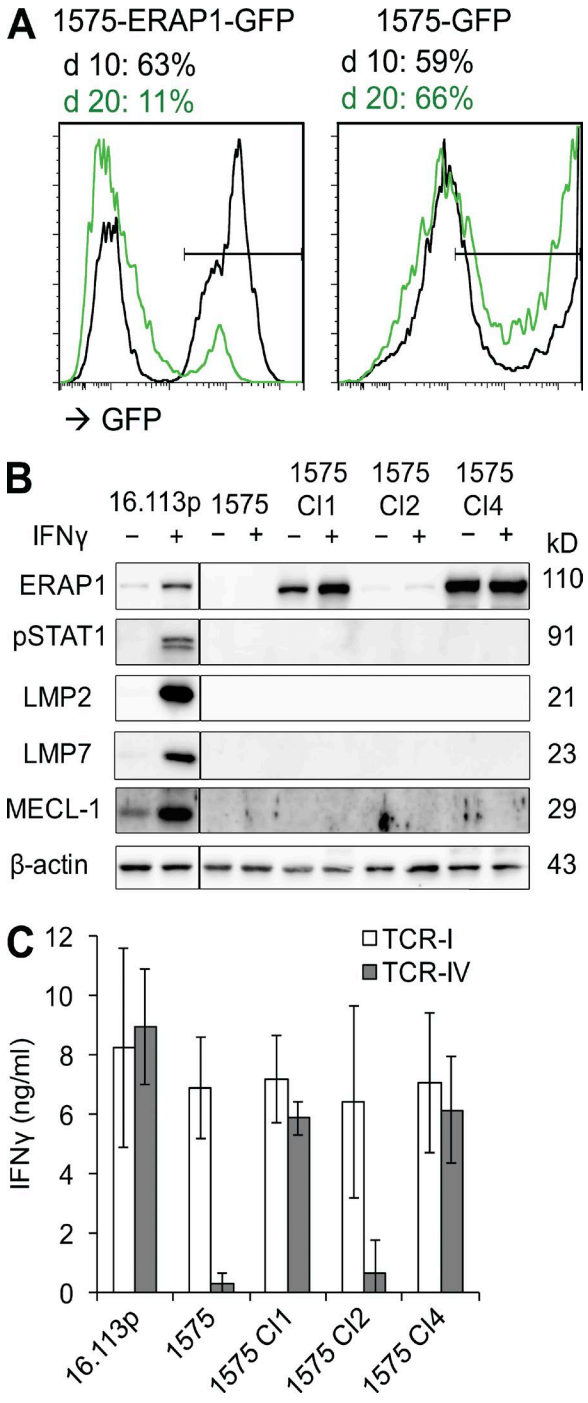

Figure 9. **Expression of ERAP1 in escape variants restores recognition by TCR-IV T cells.** (A) 1575 cells were transduced with either pMP71-ERAP1-IRES-GFP or pMP71-IRES-GFP and GFP sorted. Histograms indicate GFP expression at days 10 and 20 after sort. (B) The picture shows ERAP1, pSTAT1, LMP2, LMP7, MECL-1, and β-actin WB (single blot) for proteins from pMP71-ERAP1-IRES-GFP stably transduced 1575 GFP-selected cell clones (Cl1, Cl2, and Cl4) compared with 1575 and 16.113p cells (±IFN-γ pretreatment; 100 ng/48 h). One representative of two experiments is shown. (C) The graph shows levels of secreted IFN-γ by TCR-I– and TCR-IV–transduced OT-1/Rag$^{-/-}$ T cells after co-culture with parental 16.113p cells, 1575, the ERAP1-overexpressing 1575 clones (Cl1 and Cl4), and the ERAP1-negative clone (Cl2) measured by ELISA (E:T/2:1). Combined data from three experiments are shown, and error bars indicate SD.

molecules for tumor stroma destruction as a prerequisite for preventing tumor recurrence by escape variants (Spiotto et al., 2004; Zhang et al., 2008; Anders and Blankenstein, 2013). TCR-I T cells rejected the MHC-I high expressing Tet-TagLuc tumors and the MHC-I low expressing 16.113p tumors. Therefore, when targeting a suitable epitope, the levels of MHC-I may not be as an important factor for cancer eradication as previously believed, which is encouraging considering that many tumors express low levels of MHC-I (Bukur et al., 2012). However, the amount of produced epitopes should be sufficiently high to compensate for the low MHC-I levels.

IFN-γ secretion by T cells was essential for tumor rejection in most analyzed models (Zhang et al., 2008; Listopad et al., 2013), probably acting in multiple ways. It needs to act on the tumor stroma to induce vasculature destruction (Qin and Blankenstein, 2000; Briesemeister et al., 2011; Schietinger et al., 2013). Its effect on the cancer cells is controversial. Some studies suggested that tumor rejection required IFN-γ responsiveness by the cancer cells (Dighe et al., 1994; Kaplan et al., 1998), whereas others suggested that IFN-γ–unresponsive cancer cells were rejected at equal levels as the IFN-γ–responsive counterparts (Mumberg et al., 1999; Qin and Blankenstein, 2000). Our data may resolve this discrepancy, as they suggest that effective pIV-targeting requires the cancer cells to respond to IFN-γ, whereas pI-targeting does not. IFN-γ action on the cancer cells was suggested to increase T cell recognition by up-regulation of MHC molecules and/or components of the proteasome (Dighe et al., 1994), notably before ERAAP was discovered (Saric et al., 2002; Serwold et al., 2002). Because the immunoproteasome appears to generate quantitatively but not qualitatively different peptides (Mishto et al., 2014), it could not explain why tumors escaped TCR-IV but not TCR-I T cells, especially because pIV as the dominant epitope is usually efficiently generated. In contrast, ERAAP generates qualitatively different peptides (Hammer et al., 2006; York et al., 2006), thus the differential amounts of pI and pIV generated in the IFN-γ–unresponsive variants allowed tumors to escape only under TCR-IV T cell pressure, indicating that IFN-γ–independent epitopes qualify as rejection epitopes if all the other parameters are met. Therefore, any cancer containing variants with loss in genes that play a role in IFN-γ signaling (Abril et al., 1998; Kaplan et al., 1998; van Hall et al., 2006; Respa et al., 2011) could result in tumor escape if the generation of the targeted epitope depended on ERAP1.

The impaired recognition of the escape variants by TCR-IV T cells was probably a result of the combined effect of overall down-regulation of IFN-γ–inducible genes

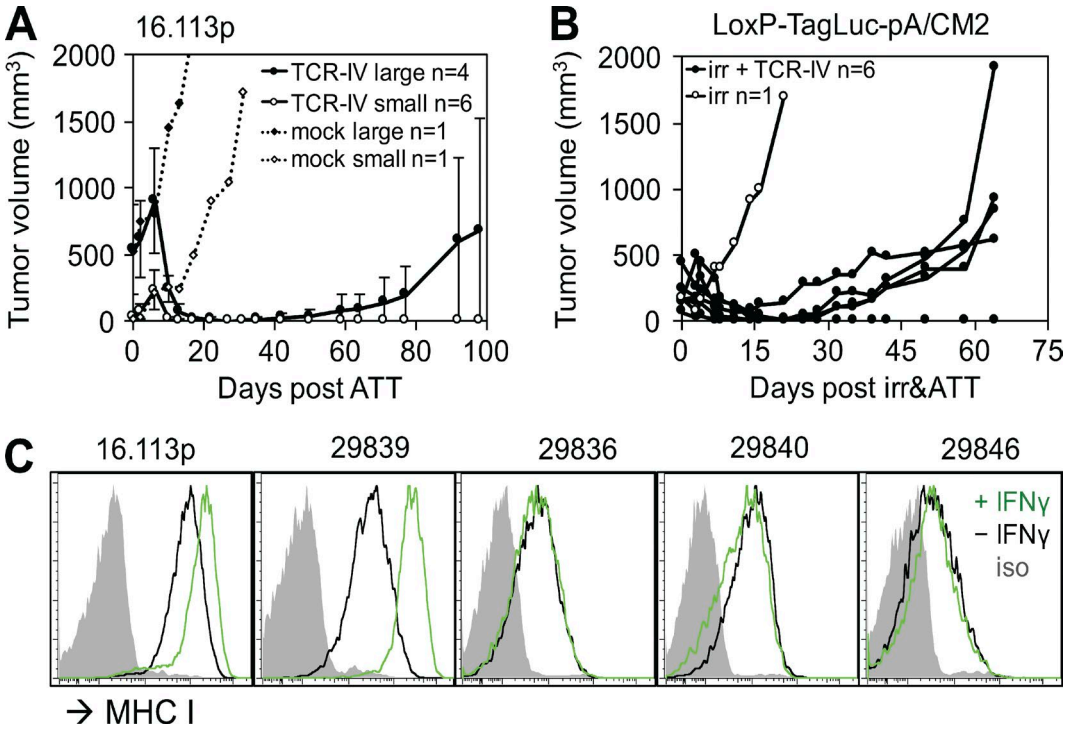

Figure 10. **Escape variants develop only in large established tumors, independent of endogenous T cells.** (A) Tumor volumes over time from $Rag^{-/-}$ mice bearing small (~10 d) and large (~30 d) 16.113p tumors that were treated on the same day with TCR-IV or mock $CD8^+$ OT-1/$Rag^{-/-}$ T cells. A single experiment is shown, and each line represents mean tumor volume of indicated mice receiving the same treatment. (B) Tumor volumes over time from LoxP-TagLuc-pA/CM2 mice bearing 16.113p tumors that received either irradiation (5 Gy) or combination of irradiation and TCR-IV T cell therapy (derived from OT-1/$Rag^{-/-}$ mice). A single experiment is shown, where each line reflects an individual mouse. (C) MHC-I expression by double staining with biotin-α-H2-K^b/D^b and streptavidin Ab, including the corresponding isotype control for untreated or IFN-γ–pretreated (100 ng/48 h) 16.113p, 29839, 29836, 29840, and 29846 (escape variant) cells. One representative staining of two is shown.

that contributed to poor epitope presentation which made them therapy resistant and allowed escape. Nevertheless, ERAP1-reconstitution in the escape variants restored TCR-IV T cell recognition, suggesting that efficient epitope IV generation was directly linked to IFN-γ–regulated postproteasomal trimming. However, the inability to up-regulate IFN-γ–inducible genes did not abolish elimination of the escape variants within 16.113p tumors when they were treated by TCR-I T cells, showing that these therapy-resistant variants still produced enough pI epitope. ERAAP deficiency leads to altered peptide pool which has been associated with increased immunogenicity (Hammer et al., 2007; James et al., 2013). Nevertheless, in our model the IFN-γ–unresponsive variants developed in established tumors independently of the presence of the endogenous T cells, suggesting that IFN-γ–resistant variants can develop naturally without causing immunogenicity.

Although the exact mechanism of escape that we see in our model has not yet been described after ATT in the clinic, a polymorphism in ERAP1 appears to be associated with poor prognosis in human papillomavirus–induced cervical carcinoma (Mehta et al., 2009). Moreover, immune escape caused by ineffective N-terminal trimming by ERAP1 has been described for HIV and CMV infections (Draenert et al., 2004; Kim et al., 2011). Therefore, when selecting rejection epitopes for ATT, it should be taken into consideration whether the epitope production is dependent on ERAP1.

MATERIALS AND METHODS

Mice

All mouse studies were in accordance with institutional, state, and federal (Landesamt für Arbeitsschutz, Gesundheitsschutz und technische Sicherheit, Berlin, Germany) guidelines. The following mice with indicated strain numbers were purchased from Taconic: $Rag^{-/-}$ (RAG2), P14 (4138; these mice were additionally backcrossed to $Rag^{-/-}$ to obtain P14/$Rag^{-/-}$ mice), OT-1/$Rag^{-/-}$ (4175) and CD45.1 (4007). ChRLuc/OT-1/$Rag^{-/-}$ mice were previously described (Charo et al., 2011), and OT-1/IFN-$\gamma^{-/-}$/$Rag^{-/-}$ were provided by T. Schüler (Institute for Molecular and Clinical Immunology, Magdeburg, Germany). LoxP-TagLuc-pA mice (Buschow et al., 2010) were crossed to CM2 mice (Anders et al., 2012) to generate LoxP-TagLuc-pA/CM2 mice. Male or female mice aged 2–8 mo were used in animal experiments.

Cells

RPMI and DMEM media (Gibco) used in cell culture were supplemented with 10% heat-inactivated FCS (PAN Biotech), 50 μg/ml gentamicin (Gibco), and 50 μM mercaptoethanol (Gibco; hereafter referred as RPMI-all and DMEM-all). Hek-T cells were used as packaging cells for retroviral vectors. MCA-205 (Anders et al., 2011) cells were used as T-Ag–negative controls. Tet-TagLuc cells were previously described (Anders et al., 2011) and 16.113p cells (16.113FP; Charo et al., 2011) were generated by one time in vivo passage of 16.113 cells (Willimsky and Blankenstein, 2005) in a P14/Rag$^{-/-}$ mouse. The seven 16.113p escape variants (999, 1004, 1575, 1577, 2100, 2106, and 2099) isolated from Rag$^{-/-}$ mice and the four 16.113p escape variants (29839, 29836, 29840, and 29846) from LoxP-TagLuc-pA/CM2 mice were generated from relapsed tumors when they reached the size of ∼500 mm^3. Tumors were excised, cut in small fragments and incubated for 6 h at 37°C in collagenase (1 mg/ml; Invitrogen) supplemented DMEM-all, after which they were cultured for 1 wk in DMEM-all supplemented with 1x antibiotic-antimycotic (Invitrogen), and then only DMEM-all was used. No routine cell line validation or mycoplasma testing was performed.

Gene vectors and transfection

TCR-I (Staveley-O'Carroll et al., 2003) and TCR-IV constructs containing α and β chains separated by the 2A element of porcine teschovirus (β-P2A-α) were designed using Vector NTI software (Invitrogen). TCR-I and TCR-IV were cloned into individual pMP71 vectors using EcoRI and NotI restriction sites. pMSCV vector encoding for GFP (pMIG) was used as mock control. Retroviral supernatants were generated by cotransfecting (1:1) ≥70% confluent Hek-T cells with pMP71-TCR-I, pMP71-TCR-IV, or mock (GFP) plasmids together with pCL-eco vector (Imgenex) using Lipofectamine 2000 (Invitrogen) according to the manufacturer's protocol. In brief, a total of 3 μg DNA was added to 500 μl OptiMEM medium (Gibco) preincubated for 5 min at RT with Lipofectamine 2000 (Invitrogen). The mix was incubated for 20 min at RT and subsequently resuspended in 1.5 ml DMEM-all and added to 6-well plate containing ≥70% confluent Hek-T cells. The cells were incubated for 8-15 h, after which the medium was replaced by RPMI-all. Supernatants were collected 48 and 72 h after transfection, filtered (0.45-μm pore size) and used in T cell transduction. ERAP1 was subcloned from pPM-hERAP1-HA (BioCat GmbH) into pMP71-IRES-GFP by NotI and SalI restriction sites, resulting in pMP71-ERAP1-IRES-GFP retroviral vector.

Expansion of T cells and retroviral transduction

Spleens were isolated from P14/Rag$^{-/-}$ or OT-1/Rag$^{-/-}$ mice and prepared as a single-cell suspension with ACK (150 mM NH_4Cl [Merck], 1 mM $KHCO_3$ [Roth], and 0.1 mM Na_2EDTA [Roth], pH 7.2) lysis of red blood cells. 1–2 × 10^6 cells were cultured in 24-well plates in 1 ml of RPMI-all supplemented with 1 μg/ml anti (α)-CD3 (clone 145-2C11), 0.1 μg/ml α-CD28 (clone 37.51) purified Ab (BD) and 10 IU/ml IL-2 (Proleukin; Prometheus Laboratories) for 24 h at 37°C in 5% CO_2 humidified incubator. After 24-h activation, media was removed from the splenocytes and replaced with 1 ml/well virus supernatant containing 10 μg/ml polybrene (Sigma-Aldrich). The cells were spinoculated for 2 h at 800 *g* and 32°C. Virus supernatant was removed and replaced with 1 ml RPMI-all containing 10 IU IL-2. Cells were transduced twice, with an interval of 24 h. The level of surface TCR expression was measured 24 or 48 h after the last transduction. Similarly, 10^6 1575 escape variant cells were plated on 6-well plates 1 d before transduction. The cells were spinoculated twice with a 24-h interval with 2 ml/well of virus supernatant (pMP71-ERAP1-IRES-GFP or pMP71-IRES-GFP) containing polybrene as described above in this paragraph. After expansion in culture (transduction ratio; ≈10% for pMP71-IRES-ERAP1-GFP) the cells were sorted for GFP and cloned.

Flow cytometry and cytokine release assays

Transduced T cells were stained with α-CD8 Ab (APC; clone 53–6.7) and the TCR cell surface expression was measured by pI- and pIV-specific PE-conjugated H2-D^b and H2-K^b tetramers (H2-D^b SAINNYAQKL and H2-K^b VVYDFLKL [anchor modified, in other assays native peptide was used]; tetramer I and tetramer IV; Beckman Coulter). Up-regulation of MHC-I on the tumor cells was obtained by incubation with 100 ng/ml IFN-γ (Gibco) for 24–48 h. MHC-I expression was measured by staining with α-H2-D^b (FITC; clone KH95; BD) and α-H2-K^b (FITC; clone AF6-88.5; BD). Alternatively, subsequent staining with biotinylated α-H-2K^b/D^b Ab (clone 28–8-6; BD) and streptavidin-APC (BD) was used to increase the MHC-I signal. 16.113p and the escape variants were stained for IFNγR by biotinylated α-CD119 Ab (clone 2E2; BD) and streptavidin-APC (BD). The signal was amplified using FASER kit (BD) according to the manufacturer's protocol. Tet-TagLuc and 16.113p cells were stained for intracellular T-Ag expression using the Cytofix/Cytoperm kit (BD) with α-T-Ag–specific Ab (FITC; PAb108; BD) according to the manufacturer's protocol. Cells derived from CD45.1 mice were identified from total splenocytes by staining with α-CD45.1 Ab (APC; clone A20; BD). For the cytokine release assay, 10^5 transduced CD8$^+$ T cells were co-cultured with 5 × 10^4 of target tumor cells (that were ≥80% confluent at the day of experiment, ±IFN-γ/48 h) in 200 μl RPMI-all media supplemented with 5 IU/ml IL-2 (Proleukin; Prometheus Laboratories) for 24 h on 37°C in 96-well plates (200 μl/well). For functional avidity, 5 × 10^4 TCR-I and TCR-IV transduced CD8$^+$ T cells were co-cultured with equal numbers of RMA-S cells pulsed with titrated amounts of freshly dissolved pI or pIV (10^{-5}–10^{-15} M). The cell supernatants from the co-cultures were tested 24 h later for cytokine levels by mouse IFN-γ ELISA kits (BD) according to the manufacturer's protocol.

Generation of reversible MHC *Strep*tamers and k_{off}-rate assay

Peptide I– and IV–specific MHC *Strep*tamers were generated using native peptides (H2-D^b SAINNYAQKL and H2-K^b VVYDFLKC, pI and pIV, respectively). To visualize monomeric pMHC-I on the surface of living T cells, a fluorochrome was conjugated to a cysteine on a linker at the end of the *Strep*tag sequences. For MHC multimerization, 1 µg of Alexa Fluor 488–conjugated MHC-I and 0.75 µg *Strep*tactin-PE were diluted in a final volume of 50 µl FACS buffer for each staining (up to 5×10^6 cells), and incubated for at least 45 min. Before MHC *Strep*tamer binding T cells were kept on ice for at least 30 min to minimize the risk of MHC *Strep*tamer internalization. Cells were subsequently resuspended in 50 µl *Strep*tamer solution and incubated on ice in the dark for 45 min after which they were stained with α-CD8 Ab (20 min) and sorted on MoFlo Legacy Cell Sorter (Beckman Coulter).

The k_{off}-rate of monomeric pMHCs from TCRs on living T cells was analyzed as previously described (Nauerth et al., 2013). In brief, cells were kept at 4°C during the whole analysis by a precooled water-cooling device, connected to a Peltier cooler. 1 µl of cells was pipetted into a reservoir built of a customized metal insert, which fitted exactly into the cooling device that was sealed with a coverslip at the bottom. To arrest cells and therefore facilitating monitoring of single cells, a polycarbonate membrane and a small metal shim were added on top of the cells. 4°C cold FACS buffer was added to the cells, the metal shim was put into the cooling device on the inverse microscope and a time series was started on the microscope, taking one picture every 10 min. By addition of D-biotin after the first picture, which diffuses through the 5-µm pore of the membrane, the MHC *Strep*tamer complex on the cells disrupts and monomeric Alexa Fluor 488–labeled p-MHC dissociate from the T cell surface. Time series were run until complete dissociation of pMHCs. Alexa Fluor 488–fluorescence intensities of single cells were background and bleaching corrected and plotted over time. To calculate the k_{off}-rate and half-life of TCR–pMHC interaction an exponential decay was fitted into the data.

Peptide competition assay

Purification of MHC molecules by affinity chromatography has been previously described (Sidney et al., 2001). Assays to quantitatively measure peptide binding to MHC-I molecules are based on the inhibition of binding of a high affinity radiolabeled peptide to purified MHC molecules, and are performed essentially as described previously (Sidney et al., 2001, 2008). In brief, 0.1–1 nM of radiolabeled peptide is coincubated at room temperature with 1 µM–1 nM of purified MHC in the presence of a cocktail of protease inhibitors and 1 µM β_2m. After a 2-d incubation, MHC-bound radioactivity is determined by capturing pMHC complexes on α-H2-K^b (clone B24-8-3) or α-H2-D^b (clone 28–14-8s) Ab-coated Lumitrac 600 plates (Greiner Bio-one), and measuring bound cpm using the TopCount (Packard Instrument Co.) microscintillation counter. In the case of competitive assays, the concentration of peptide yielding 50% inhibition of the binding of the radiolabeled peptide is calculated. Under the conditions used, where [label]<[MHC] and $IC_{50} \geq$ [MHC], the measured IC_{50} values are reasonable approximations of the true kD values (Cheng and Prusoff, 1973; Gulukota et al., 1997). Each competitor peptide (H2-D^b–specific SAINNYAQKL and H2-K^b–specific VVYDFLKC, pI and pIV, respectively) was tested at six different concentrations covering a 100,000-fold dose range, and in three or more independent experiments. As a positive control, unlabeled version of the radiolabeled probe was also tested in each experiment. The indicator peptides used were Adenovirus E1A P7>Y (SGPSNTYPEI) for H2-D^b and VSV NP_{52-59} (RGYVFQGL) for H2-K^b.

In vivo kill assay

1 wk before the assay, C57BL/6 mice were immunized by i.p. injection of 10^7 16.113 cells resuspended in 100 µl PBS to be used as positive controls. Spleen was isolated from a CD45.1 mouse and single-cell suspension was prepared. After red blood cell lysis with ACK buffer for 2 min, splenocytes were washed twice with 1x PBS (Gibco) and divided into three tubes. The cells were either left untreated or incubated with pI or anchor-modified pIV (VVYDFLKL), at a final concentration of 0.5 µM at 37°C for 30 min. Subsequently, the three populations were labeled with different concentration of CFSE (Invitrogen) and incubated at 37°C for 15 min. The final CFSE concentration was 0.025, 0.25, and 2.5 µM for unpulsed, pI-, and pIV-pulsed cells, respectively. The cells were washed three times with PBS, the different populations were mixed at 1:1:1 ratio, and $5–10 \times 10^6$ cells in 100 µl PBS were i.v. injected into the mice. 16 h later, spleens were isolated and splenocytes were stained with α-CD45.1 Ab and analyzed by flow cytometry.

WB

Cells were lysed in 50 mM Tris-HCl (pH 7.5), 50 mM NaCl, 5 mM $MgCl_2$, 0.1% Triton X-100, and protease inhibitor (cOmplete; Roche). 20 µg of total protein extracts were separated by SDS-PAGE and transferred onto a nitrocellulose membrane (Optitran BA-S 85 Reinforced NC; Whatman). The membrane was incubated in PBS supplemented with 0.4% Tween-20 and 5% dry milk for 1 h. Primary antibodies recognizing Jak1 (6G4; Cell Signaling Technology), Jak2 (D2E12; Cell Signaling Technology), Stat1 (polyclonal; Cell Signaling Technology), Phospho-Stat1 (58D6 [Tyr701]; Cell Signaling Technology), ERAP1 (6H9), MECL (K6512), LMP2 (polyclonal; Abcam), LMP7 (polyclonal; Abcam), or β-Actin (C4; Santa Cruz Biotechnology, Inc.) were diluted in PBS/0.1% Tween-20 and 2.5% dry milk and were applied overnight at 4°C. The membrane was washed three times with PBS/0.1% Tween-20 followed by 1-h incubation with the secondary Ab (0.2 µg/ml goat anti–rabbit IgG H&L chain–specific peroxidase conjugate, rabbit anti–mouse IgG

H&L chain–specific peroxidase conjugate, or rabbit anti–goat IgG H&L chain–specific peroxidase conjugate; EMD Millipore). The ECL Prime Western Blotting Detection kit (GE Healthcare) was used for detection. Membranes were analyzed with the Fusion FX System using FusionCapt Advance FX7 Software (Peqlab).

Tumor challenge and adoptive T cell transfer

Age- and sex-matched mice were injected s.c. into the right flank with 5×10^6 tumor cells in 100 µl PBS. On the day of ATT, mice were ranked by tumor size and equal mean tumor sizes were allocated to different therapy groups. Mice received 5×10^4 or 5×10^5 $CD8^+$ T cells in 100 µl PBS i.v. Tumor size was measured by caliper, and the mean tumor size was determined from the measurements along three orthogonal axes (a, b, and c). Tumor volumes were calculated according to this formula: $V\ (mm^3) = (a \times b \times c)/2$. Mice were sacrificed when the tumors reached 15 mm mean diameter. Animals were excluded from analysis if they died from reasons unrelated to tumor burden, and the experimenter was not blinded with respect to treatment groups. No prespecified effect size was used to determine sample sizes in animal studies.

Bioluminescence imaging

In vivo imaging was performed using a Xenogen IVIS 200 (Caliper Lifescience). A maximum of five anesthetized mice were imaged at once. Each mouse received an i.v. injection of freshly prepared coelenterazine (Biosynth) that was dissolved in DMSO (Sigma-Aldrich) and diluted in PBS (100 µg/100 µl per mouse; Charo et al., 2011). Images were acquired for 1 min using small binning. All data were analyzed using Living Image analysis software (Caliper Lifescience). The region of interest for the measured signal was drawn at the tumor site identically for all mice and was set anew for each experiment.

Proteasomal isolation, peptide cleavage, and mass spectrometry (MS)

20S proteasomes were purified from T2, T2.27, or lymphoblastoid cell lines as previously reported (Theobald et al., 1998) and the purity was verified by SDS-PAGE electrophoresis (12.5% poly-acrylamide gel stained with Coomassie dye). Synthetic peptides at different concentrations (from 20 to 80 µM) were digested by 1–5 µg 20S proteasomes in 100 µl TEAD buffer (20 mM Tris, 1 mM EDTA, 1 mM sodium azide, and 1 mM dithiothreitol, pH 7.2) for different time periods (from 1 to 24 h) at 37°C. Digestions were stopped with 0.1 vol of trifluoroacetic acid and frozen. All experiments were repeated at least twice. In liquid chromatography runs, the peptide separation was performed on a 1 mm RP column (Beta Basic-18, 100 mm × 1 mm, 3 mm, 150 Å; Thermo Fisher Scientific) using a Surveyor system (Thermo Fisher Scientific). The mobile phase (A) was 100% water containing 0.05% (vol/vol) trifluoroacetic acid, and (B) was 70:30 (vol/vol) acetonitrile/water containing 0.045% (vol/vol) trifluoroacetic acid. The elution was performed on binary gradient: 3% B 10 min, 3–63% B in 32 min. A flow rate of 30 µl/min was used. Online MS analysis was performed by DECA XP MAX iontrap instrument (Thermo Fisher Scientific). MS data were acquired with a triple scan method in positive ion mode (MS: mass range, 200–2000 m/z; zoom scan, MS/MS). Analysis of ESI/MS data were accomplished using Bioworks version 3.3 (Thermo Fisher Scientific). Database searching was performed using the following parameters: no enzyme, mass tolerance for fragment ions 1.5 amu (atomic mass unit). In time-dependent processing experiments (signal intensity versus time of digestion) the kinetics of the identified peaks was analyzed by using LCQuan software version 2.5 (Thermo Fisher Scientific).

Statistics

Statistical analysis was performed on data obtained with k_{off}-rate assay. Sample groups were compared using a two-sided Wilcoxon rank sum test. The variances of the two groups were compared by F-test and were not equal (p-value = 0.039).

Online supplemental material

Fig. S1 shows low H-2/D^b/K^b expression on escape variants that cannot be up-regulated with IFN-γ despite surface IFNγR. Fig. S2 shows TCR-IV escape variants are IFN-γ unresponsive and not recognized in vitro. Fig. S3 describes immunoproteasome cleavage products of T-$Ag_{196-221}$ and T-$Ag_{398-417}$.

ACKNOWLEDGMENTS

The authors would like to thank E. Kieback for her input in vector design, T. Schüler for providing OT-1/IFN-$\gamma^{-/-}$/$Rag^{-/-}$ mice, Rosa Karlić for statistical analysis, and M. Hensel, S. Kupsch, and M. Babka for technical assistance.

This work was supported by the Deutsche Forschungsgemeinschaft through Sonderforschungsbereich TR36, SFB854 and the Berlin Institute of Health.

The authors declare no competing financial interests.

Author contributions: A. Textor, K. Schmidt, B. Weißbrich, C. Perez, J. Sidney, and C. Keller performed research; J. Charo, K. Anders, C. Perez, and T.N.M. Schumacher provided reagents and gave advice; A. Textor, K. Schmidt, P.-M. Kloetzel, B. Weißbrich, C. Perez, J. Sidney, A. Sette, C. Keller, D.H. Busch, U. Seifert, and T. Blankenstein analyzed data; A. Textor and T. Blankenstein developed the study and wrote the manuscript. All authors revised the manuscript.

Submitted: 3 May 2016
Accepted: 31 August 2016

REFERENCES

Abril, E., L.M. Real, A. Serrano, P. Jimenez, A. García, J. Canton, I. Trigo, F. Garrido, and F. Ruiz-Cabello. 1998. Unresponsiveness to interferon associated with STAT1 protein deficiency in a gastric adenocarcinoma cell line. *Cancer Immunol. Immunother.* 47:113–120. http://dx.doi.org/10.1007/s002620050511

Anders, K., and T. Blankenstein. 2013. Molecular pathways: comparing the effects of drugs and T cells to effectively target oncogenes. *Clin. Cancer Res.* 19:320–326. http://dx.doi.org/10.1158/1078-0432.CCR-12-3017

Anders, K., C. Buschow, A. Herrmann, A. Milojkovic, C. Loddenkemper, T. Kammertoens, P. Daniel, H. Yu, J. Charo, and T. Blankenstein. 2011. Oncogene-targeting T cells reject large tumors while oncogene inactivation selects escape variants in mouse models of cancer. *Cancer Cell.* 20:755–767. http://dx.doi.org/10.1016/j.ccr.2011.10.019

Anders, K., C. Buschow, J. Charo, and T. Blankenstein. 2012. Depot formation of doxycycline impairs Tet-regulated gene expression in vivo. *Transgenic Res.* 21:1099–1107. http://dx.doi.org/10.1007/s11248-011-9580-0

Androlewicz, M.J., K.S. Anderson, and P. Cresswell. 1993. Evidence that transporters associated with antigen processing translocate a major histocompatibility complex class I-binding peptide into the endoplasmic reticulum in an ATP-dependent manner. *Proc. Natl. Acad. Sci. USA.* 90:9130–9134. http://dx.doi.org/10.1073/pnas.90.19.9130

Bendle, G.M., C. Linnemann, L. Bies, J.-Y. Song, and T.N.M. Schumacher. 2013. Blockade of TGF-β signaling greatly enhances the efficacy of TCR gene therapy of cancer. *J. Immunol.* 191:3232–3239. http://dx.doi.org/10.4049/jimmunol.1301270

Briesemeister, D., D. Sommermeyer, C. Loddenkemper, R. Loew, W. Uckert, T. Blankenstein, and T. Kammertoens. 2011. Tumor rejection by local interferon gamma induction in established tumors is associated with blood vessel destruction and necrosis. *Int. J. Cancer.* 128:371–378. http://dx.doi.org/10.1002/ijc.25350

Bukur, J., S. Jasinski, and B. Seliger. 2012. The role of classical and non-classical HLA class I antigens in human tumors. *Semin. Cancer Biol.* 22:350–358. http://dx.doi.org/10.1016/j.semcancer.2012.03.003

Buschow, C., J. Charo, K. Anders, C. Loddenkemper, A. Jukica, W. Alsamah, C. Perez, G. Willimsky, and T. Blankenstein. 2010. In vivo imaging of an inducible oncogenic tumor antigen visualizes tumor progression and predicts CTL tolerance. *J. Immunol.* 184:2930–2938. http://dx.doi.org/10.4049/jimmunol.0900893

Chang, C.-C., and S. Ferrone. 2007. Immune selective pressure and HLA class I antigen defects in malignant lesions. *Cancer Immunol. Immunother.* 56:227–236. http://dx.doi.org/10.1007/s00262-006-0183-1

Charo, J., C. Perez, C. Buschow, A. Jukica, M. Czeh, and T. Blankenstein. 2011. Visualizing the dynamic of adoptively transferred T cells during the rejection of large established tumors. *Eur. J. Immunol.* 41:3187–3197. http://dx.doi.org/10.1002/eji.201141452

Cheng, Y., and W.H. Prusoff. 1973. Relationship between the inhibition constant (K1) and the concentration of inhibitor which causes 50 per cent inhibition (I50) of an enzymatic reaction. *Biochem. Pharmacol.* 22:3099–3108. http://dx.doi.org/10.1016/0006-2952(73)90196-2

Cormier, J.N., M.C. Panelli, J.A. Hackett, M.P. Bettinotti, A. Mixon, J. Wunderlich, L.L. Parker, N.P. Restifo, S. Ferrone, and F.M. Marincola. 1999. Natural variation of the expression of HLA and endogenous antigen modulates CTL recognition in an in vitro melanoma model. *Int. J. Cancer.* 80:781–790. http://dx.doi.org/10.1002/(SICI)1097-0215(19990301)80:5<781::AID-IJC24>3.0.CO;2-A

Dighe, A.S., E. Richards, L.J. Old, and R.D. Schreiber. 1994. Enhanced in vivo growth and resistance to rejection of tumor cells expressing dominant negative IFN gamma receptors. *Immunity.* 1:447–456. http://dx.doi.org/10.1016/1074-7613(94)90087-6

Draenert, R., S. Le Gall, K.J. Pfafferott, A.J. Leslie, P. Chetty, C. Brander, E.C. Holmes, S.-C. Chang, M.E. Feeney, M.M. Addo, et al. 2004. Immune selection for altered antigen processing leads to cytotoxic T lymphocyte escape in chronic HIV-1 infection. *J. Exp. Med.* 199:905–915. http://dx.doi.org/10.1084/jem.20031982

Dunn, G.P., K.C.F. Sheehan, L.J. Old, and R.D. Schreiber. 2005. IFN unresponsiveness in LNCaP cells due to the lack of JAK1 gene expression. *Cancer Res.* 65:3447–3453. http://dx.doi.org/10.1158/0008-5472.CAN-04-4316

Engels, B., V.H. Engelhard, J. Sidney, A. Sette, D.C. Binder, R.B. Liu, D.M. Kranz, S.C. Meredith, D.A. Rowley, and H. Schreiber. 2013. Relapse or eradication of cancer is predicted by peptide-major histocompatibility complex affinity. *Cancer Cell.* 23:516–526. http://dx.doi.org/10.1016/j.ccr.2013.03.018

Feenstra, M., M. Veltkamp, J. van Kuik, S. Wiertsema, P. Slootweg, J. van den Tweel, R. de Weger, and M. Tilanus. 1999. HLA class I expression and chromosomal deletions at 6p and 15q in head and neck squamous cell carcinomas. *Tissue Antigens.* 54:235–245. http://dx.doi.org/10.1034/j.1399-0039.1999.540304.x

Gallimore, A., T. Dumrese, H. Hengartner, R.M. Zinkernagel, and H.-G. Rammensee. 1998. Protective immunity does not correlate with the hierarchy of virus-specific cytotoxic T cell responses to naturally processed peptides. *J. Exp. Med.* 187:1647–1657. http://dx.doi.org/10.1084/jem.187.10.1647-b

Garbi, N., B. Arnold, S. Gordon, G.J. Hämmerling, and R. Ganss. 2004. CpG motifs as proinflammatory factors render autochthonous tumors permissive for infiltration and destruction. *J. Immunol.* 172:5861–5869. http://dx.doi.org/10.4049/jimmunol.172.10.5861

Garrido, C., L. Paco, I. Romero, E. Berruguilla, J. Stefansky, A. Collado, I. Algarra, F. Garrido, and A.M. Garcia-Lora. 2012. MHC class I molecules act as tumor suppressor genes regulating the cell cycle gene expression, invasion and intrinsic tumorigenicity of melanoma cells. *Carcinogenesis.* 33:687–693. http://dx.doi.org/10.1093/carcin/bgr318

Gulukota, K., J. Sidney, A. Sette, and C. DeLisi. 1997. Two complementary methods for predicting peptides binding major histocompatibility complex molecules. *J. Mol. Biol.* 267:1258–1267. http://dx.doi.org/10.1006/jmbi.1997.0937

Hammer, G.E., F. Gonzalez, M. Champsaur, D. Cado, and N. Shastri. 2006. The aminopeptidase ERAAP shapes the peptide repertoire displayed by major histocompatibility complex class I molecules. *Nat. Immunol.* 7:103–112. http://dx.doi.org/10.1038/ni1286

Hammer, G.E., F. Gonzalez, E. James, H. Nolla, and N. Shastri. 2007. In the absence of aminopeptidase ERAAP, MHC class I molecules present many unstable and highly immunogenic peptides. *Nat. Immunol.* 8:101–108. http://dx.doi.org/10.1038/ni1409

James, E., I. Bailey, G. Sugiyarto, and T. Elliott. 2013. Induction of protective antitumor immunity through attenuation of ERAAP function. *J. Immunol.* 190:5839–5846. http://dx.doi.org/10.4049/jimmunol.1300220

Kaplan, D.H., V. Shankaran, A.S. Dighe, E. Stockert, M. Aguet, L.J. Old, and R.D. Schreiber. 1998. Demonstration of an interferon γ-dependent tumor surveillance system in immunocompetent mice. *Proc. Natl. Acad. Sci. USA.* 95:7556–7561. http://dx.doi.org/10.1073/pnas.95.13.7556

Kim, S., S. Lee, J. Shin, Y. Kim, I. Evnouchidou, D. Kim, Y.-K. Kim, Y.-E. Kim, J.-H. Ahn, S.R. Riddell, et al. 2011. Human cytomegalovirus microRNA miR-US4-1 inhibits $CD8^+$ T cell responses by targeting the aminopeptidase ERAP1. *Nat. Immunol.* 12:984–991. http://dx.doi.org/10.1038/ni.2097

Kloetzel, P.M., and F. Ossendorp. 2004. Proteasome and peptidase function in MHC-class-I-mediated antigen presentation. *Curr. Opin. Immunol.* 16:76–81. http://dx.doi.org/10.1016/j.coi.2003.11.004

Leal, J.F., J. Fominaya, A. Cascón, M.V. Guijarro, C. Blanco-Aparicio, M. Lleonart, M.E. Castro, S. Ramon Y Cajal, M. Robledo, D.H. Beach, and A. Carnero. 2008. Cellular senescence bypass screen identifies new putative tumor suppressor genes. *Oncogene.* 27:1961–1970. http://dx.doi.org/10.1038/sj.onc.1210846

Listopad, J.J., T. Kammertoens, K. Anders, B. Silkenstedt, G. Willimsky, K. Schmidt, A.A. Kuehl, C. Loddenkemper, and T. Blankenstein. 2013. Fas expression by tumor stroma is required for cancer eradication. *Proc. Natl. Acad. Sci. USA.* 110:2276–2281. http://dx.doi.org/10.1073/pnas.1218295110

Lyman, M.A., C.T. Nugent, K.L. Marquardt, J.A. Biggs, E.G. Pamer, and L.A. Sherman. 2005. The fate of low affinity tumor-specific $CD8^+$ T cells in tumor-bearing mice. *J. Immunol.* 174:2563–2572. http://dx.doi.org/10.4049/jimmunol.174.5.2563

Mackensen, A., N. Meidenbauer, S. Vogl, M. Laumer, J. Berger, and R. Andreesen. 2006. Phase I study of adoptive T-cell therapy using antigen-specific $CD8^+$ T cells for the treatment of patients with metastatic

melanoma. *J. Clin. Oncol.* 24:5060–5069. http://dx.doi.org/10.1200/JCO.2006.07.1100

Mehta, A.M., E.S. Jordanova, W.E. Corver, T. van Wezel, H.-W. Uh, G.G. Kenter, and G. Jan Fleuren. 2009. Single nucleotide polymorphisms in antigen processing machinery component ERAP1 significantly associate with clinical outcome in cervical carcinoma. *Genes Chromosomes Cancer.* 48:410–418. http://dx.doi.org/10.1002/gcc.20648

Mishto, M., J. Liepe, K. Textoris-Taube, C. Keller, P. Henklein, M. Weberruß, B. Dahlmann, C. Enenkel, A. Voigt, U. Kuckelkorn, et al. 2014. Proteasome isoforms exhibit only quantitative differences in cleavage and epitope generation. *Eur. J. Immunol.* 44:3508–3521. http://dx.doi.org/10.1002/eji.201444902

Mumberg, D., P.A. Monach, S. Wanderling, M. Philip, A.Y. Toledano, R.D. Schreiber, and H. Schreiber. 1999. CD4(+) T cells eliminate MHC class II-negative cancer cells in vivo by indirect effects of IFN-gamma. *Proc. Natl. Acad. Sci. USA.* 96:8633–8638. http://dx.doi.org/10.1073/pnas.96.15.8633

Mylin, L.M., T.D. Schell, D. Roberts, M. Epler, A. Boesteanu, E.J. Collins, J.A. Frelinger, S. Joyce, and S.S. Tevethia. 2000. Quantitation of $CD8^+$ T-lymphocyte responses to multiple epitopes from simian virus 40 (SV40) large T antigen in C57BL/6 mice immunized with SV40, SV40 T-antigen-transformed cells, or vaccinia virus recombinants expressing full-length T antigen or epitope minigenes. *J. Virol.* 74:6922–6934. http://dx.doi.org/10.1128/JVI.74.15.6922-6934.2000

Nauerth, M., B. Weißbrich, R. Knall, T. Franz, G. Dössinger, J. Bet, P.J. Paszkiewicz, L. Pfeifer, M. Bunse, W. Uckert, et al. 2013. TCR-ligand koff rate correlates with the protective capacity of antigen-specific $CD8^+$ T cells for adoptive transfer. *Sci. Transl. Med.* 5:192ra87. http://dx.doi.org/10.1126/scitranslmed.3005958

Otahal, P., B.B. Knowles, S.S. Tevethia, and T.D. Schell. 2007. Anti-CD40 conditioning enhances the T(CD8) response to a highly tolerogenic epitope and subsequent immunotherapy of simian virus 40 T antigen-induced pancreatic tumors. *J. Immunol.* 179:6686–6695. http://dx.doi.org/10.4049/jimmunol.179.10.6686

Paschen, A., R.M. Méndez, P. Jimenez, A. Sucker, F. Ruiz-Cabello, M. Song, F. Garrido, and D. Schadendorf. 2003. Complete loss of HLA class I antigen expression on melanoma cells: a result of successive mutational events. *Int. J. Cancer.* 103:759–767. http://dx.doi.org/10.1002/ijc.10906

Qin, Z., and T. Blankenstein. 2000. $CD4^+$ T cell–mediated tumor rejection involves inhibition of angiogenesis that is dependent on IFNγ receptor expression by nonhematopoietic cells. *Immunity.* 12:677–686. http://dx.doi.org/10.1016/S1074-7613(00)80218-6

Respa, A., J. Bukur, S. Ferrone, G. Pawelec, Y. Zhao, E. Wang, F.M. Marincola, and B. Seliger. 2011. Association of IFN-gamma signal transduction defects with impaired HLA class I antigen processing in melanoma cell lines. *Clin. Cancer Res.* 17:2668–2678. http://dx.doi.org/10.1158/1078-0432.CCR-10-2114

Restifo, N.P., F.M. Marincola, Y. Kawakami, J. Taubenberger, J.R. Yannelli, and S.A. Rosenberg. 1996. Loss of functional beta 2-microglobulin in metastatic melanomas from five patients receiving immunotherapy. *J. Natl. Cancer Inst.* 88:100–108. http://dx.doi.org/10.1093/jnci/88.2.100

Rock, K.L., C. Gramm, L. Rothstein, K. Clark, R. Stein, L. Dick, D. Hwang, and A.L. Goldberg. 1994. Inhibitors of the proteasome block the degradation of most cell proteins and the generation of peptides presented on MHC class I molecules. *Cell.* 78:761–771. http://dx.doi.org/10.1016/S0092-8674(94)90462-6

Rosenberg, S.A., J.C. Yang, R.M. Sherry, U.S. Kammula, M.S. Hughes, G.Q. Phan, D.E. Citrin, N.P. Restifo, P.F. Robbins, J.R. Wunderlich, et al. 2011. Durable complete responses in heavily pretreated patients with metastatic melanoma using T-cell transfer immunotherapy. *Clin. Cancer Res.* 17:4550–4557. http://dx.doi.org/10.1158/1078-0432.CCR-11-0116

Saric, T., S.-C. Chang, A. Hattori, I.A. York, S. Markant, K.L. Rock, M. Tsujimoto, and A.L. Goldberg. 2002. An IFN-gamma-induced aminopeptidase in the ER, ERAP1, trims precursors to MHC class I-presented peptides. *Nat. Immunol.* 3:1169–1176. http://dx.doi.org/10.1038/ni859

Schietinger, A., A. Arina, R.B. Liu, S. Wells, J. Huang, B. Engels, V. Bindokas, T. Bartkowiak, D. Lee, A. Herrmann, et al. 2013. Longitudinal confocal microscopy imaging of solid tumor destruction following adoptive T cell transfer. *OncoImmunology.* 2:e26677. http://dx.doi.org/10.4161/onci.26677

Serwold, T., F. Gonzalez, J. Kim, R. Jacob, and N. Shastri. 2002. ERAAP customizes peptides for MHC class I molecules in the endoplasmic reticulum. *Nature.* 419:480–483. http://dx.doi.org/10.1038/nature01074

Sidney, J., S. Southwood, C. Oseroff, M.F. del Guercio, A. Sette, and H.M. Grey. 2001. Measurement of MHC/peptide interactions by gel filtration. *Curr. Protoc. Immunol.* Chapter 18:3.

Sidney, J., E. Assarsson, C. Moore, S. Ngo, C. Pinilla, A. Sette, and B. Peters. 2008. Quantitative peptide binding motifs for 19 human and mouse MHC class I molecules derived using positional scanning combinatorial peptide libraries. *Immunome Res.* 4:2. http://dx.doi.org/10.1186/1745-7580-4-2

Spiotto, M.T., D.A. Rowley, and H. Schreiber. 2004. Bystander elimination of antigen loss variants in established tumors. *Nat. Med.* 10:294–298. http://dx.doi.org/10.1038/nm999

Staveley-O'Carroll, K., T.D. Schell, M. Jimenez, L.M. Mylin, M.J. Tevethia, S.P. Schoenberger, and S.S. Tevethia. 2003. In vivo ligation of CD40 enhances priming against the endogenous tumor antigen and promotes $CD8^+$ T cell effector function in SV40 T antigen transgenic mice. *J. Immunol.* 171:697–707. http://dx.doi.org/10.4049/jimmunol.171.2.697

Suh, W.K., M.F. Cohen-Doyle, K. Fruh, K. Wang, P.A. Peterson, and D.B. Williams. 1994. Interaction of MHC class I molecules with the transporter associated with antigen processing. *Science.* 264:1322–1326. http://dx.doi.org/10.1126/science.8191286

Theobald, M., J. Biggs, D. Dittmer, A.J. Levine, and L.A. Sherman. 1995. Targeting p53 as a general tumor antigen. *Proc. Natl. Acad. Sci. USA.* 92:11993–11997. http://dx.doi.org/10.1073/pnas.92.26.11993

Theobald, M., T. Ruppert, U. Kuckelkorn, J. Hernandez, A. Häussler, E.A. Ferreira, U. Liewer, J. Biggs, A.J. Levine, C. Huber, et al. 1998. The sequence alteration associated with a mutational hotspot in p53 protects cells from lysis by cytotoxic T lymphocytes specific for a flanking peptide epitope. *J. Exp. Med.* 188:1017–1028. http://dx.doi.org/10.1084/jem.188.6.1017

Ungureanu, D., P. Saharinen, I. Junttila, D.J. Hilton, and O. Silvennoinen. 2002. Regulation of Jak2 through the ubiquitin-proteasome pathway involves phosphorylation of Jak2 on Y1007 and interaction with SOCS-1. *Mol. Cell. Biol.* 22:3316–3326. http://dx.doi.org/10.1128/MCB.22.10.3316-3326.2002

van Hall, T., E.Z. Wolpert, P. van Veelen, S. Laban, M. van der Veer, M. Roseboom, S. Bres, P. Grufman, A. de Ru, H. Meiring, et al. 2006. Selective cytotoxic T-lymphocyte targeting of tumor immune escape variants. *Nat. Med.* 12:417–424. http://dx.doi.org/10.1038/nm1381

Weimershaus, M., I. Evnouchidou, L. Saveanu, and P. van Endert. 2013. Peptidases trimming MHC class I ligands. *Curr. Opin. Immunol.* 25:90–96. http://dx.doi.org/10.1016/j.coi.2012.10.001

Willimsky, G., and T. Blankenstein. 2005. Sporadic immunogenic tumours avoid destruction by inducing T-cell tolerance. *Nature.* 437:141–146. http://dx.doi.org/10.1038/nature03954

Yee, C., J.A. Thompson, D. Byrd, S.R. Riddell, P. Roche, E. Celis, and P.D. Greenberg. 2002. Adoptive T cell therapy using antigen-specific $CD8^+$

T cell clones for the treatment of patients with metastatic melanoma: in vivo persistence, migration, and antitumor effect of transferred T cells. *Proc. Natl. Acad. Sci. USA.* 99:16168–16173. http://dx.doi.org/10.1073/pnas.242600099

York, I.A., M.A. Brehm, S. Zendzian, C.F. Towne, and K.L. Rock. 2006. Endoplasmic reticulum aminopeptidase 1 (ERAP1) trims MHC class I-presented peptides in vivo and plays an important role in immunodominance. *Proc. Natl. Acad. Sci. USA.* 103:9202–9207. http://dx.doi.org/10.1073/pnas.0603095103

Yu, P., D.A. Rowley, Y.-X. Fu, and H. Schreiber. 2006. The role of stroma in immune recognition and destruction of well-established solid tumors. *Curr. Opin. Immunol.* 18:226–231. http://dx.doi.org/10.1016/j.coi.2006.01.004

Zhang, B., T. Karrison, D.A. Rowley, and H. Schreiber. 2008. IFN-gamma- and TNF-dependent bystander eradication of antigen-loss variants in established mouse cancers. *J. Clin. Invest.* 118:1398–1404. http://dx.doi.org/10.1172/JCI33522